2011 International Nuclear Atlantic Conference - INAC 2011
Belo Horizonte,MG, Brazil, October 24-28, 2011
ASSOCIAÇÃO BRASILEIRA DE ENERGIA NUCLEAR - ABEN
ISBN: **978-85-99141-04-5**

MULTIELEMENTAR SEGREGATION ANALYSIS OF THE THALLIUM BROMIDE IMPURITIES PURIFIED BY REPEATED BRIDGMAN TECHNIQUE

Robinson A. dos Santos[1], Fabio E. da Costa, Roseli F. Gennari[2] , João F.T. Martins, Renata M. Marcondes, Carlos H. de Mesquita, Margarida M. Hamada[3]

[1,3]Instituto de Pesquisas Energéticas e Nucleares (IPEN / CNEN - SP)
Av. Professor Lineu Prestes 2242
05508-000, Cidade Universitária, São Paulo - Brasil
[2]Instituto de Física – Universidade de São Paulo (IF-USP)
Rua do Matão Travessa R, 187
05508-090, Cidade Universitária, São Paulo - Brasil

[1]rasantos@ipen.br, [3]mmhamada@ipen.br

ABSTRACT

TlBr crystals were purified and grown by the repeated Bridgman method from two commercial TlBr salts and characterized to be used as radiation detectors. To evaluate the purification efficiency, measurements of the impurity concentration were made after each growth, analyzing the trace impurities by inductively coupled plasma mass spectroscopy (ICP-MS). A significant decrease of the impurity concentration resulting from the purification number was observed. To evaluate the crystal as a radiation semiconductor detector, measurements of its resistivity and gamma-ray spectroscopy were carried out. The radiation response depended on the crystal purity. The repeated Bridgman technique improved the TlBr crystal quality used as a radiation detector. A compartmental model was proposed to fit the impurity concentration as a function of the repetition number of the Bridgman growth.

Keywords: Thallium bromide; Semiconductor detector; Crystal Growth; Compartmental analysis.

1. INTRODUCTION

The main physical semiconductor properties required for the production of room temperature semiconductor detectors are: (a) high atomic number and density for high stopping power; (b) band gap large enough to maintain leakage currents low at room temperature and (c) large mobility−lifetime products ($\mu\tau$) for electrons and holes aiming efficient charge collection [1,2]. TlBr has emerged as a particularly interesting material as room temperature semiconductor in view of its wide band gap (2.68 eV) and its large density (7.5 g/cm^3). TlBr crystals are composed of high atomic number elements (Z_{Tl}=81 and Z_{Br}=35) and show high resistivity (>$10^{10}\Omega$cm) [2-8]. These are important factors in applications where compact and small thickness detectors are necessary for X- and gamma ray measurements [2].

The performance of a radiation semiconductor detector depends on several factors related to the crystal quality, such as the carrier lifetime, mobility, crystallographic imperfections and the impurity concentrations present in the crystal. Several studies on the preparation of TlBr

detectors have been carried out and improvements in the methodology of purification, growth and characterization of the crystals have been described, aiming to achieve all these factors [2-7]. However, as it can be observed in the literature [1,8-12], the TlBr detector limitations are not yet completely resolved: primarily, the low collection efficiency of charge carriers, fact that is probably caused by impurities and defects created in the crystal growth or in the surface treatment process. There is a consensus in the literature that the TlBr crystal purity is a crucial factor for its optimal performance as a radiation detector [2-6].

In this work, some aspects of the crystal impurity influence on the detector performance were evaluated, by systematic measurements of the gamma-ray spectrometry and resistivity. To purify the crystal, the crystal was grown by the Bridgman technique three times. The impurity decrease in the crystal was evaluated after each repetition number of the crystal growth using the ICP-MS technique. The theory of compartments was used as a mathematical model to explain and to fit the data of the impurity concentration as a function of the crystal growth repetition number.

2. MATERIAL AND METHODS

Two commercially available TlBr salts (Aldrich-Sigma and Merck, in alphabetical order), with nominal purity of 99.99%, were used as the raw salt for crystal growths. In this work, the crystals were named salt 1 and salt 2, but for the sake of business ethics, the results presented here do not identify their origin. TlBr crystals were grown by the vertical Bridgman technique, using quartz tubes as crucibles in vacuum atmosphere. Preliminary, the quartz tubes were submitted to a chemical treatment. The tubes were previously washed with a cleaning agent solution (Extran MA 02, Merck) and, then, filled with a solution of hydrofluoric acid (5 per cent v/v); after 20 minutes, the tubes were rinsed three times with demineralized water. Subsequently, the quartz tubes were submitted to a thermal treatment at 250 ºC to avoid the adhesion of the crystals on the walls of the tubes. Afterward, the TlBr salt was introduced into one tube, evacuated to 10^{-6} Torr and sealed off. The tube with TlBr was mounted into the vertical Bridgman furnace where the TlBr was melted at a temperature of 560 ºC. Crystals around 20 mm diameter and 60 mm long were obtained, with a growth rate of 1 mm/h. Following the same procedure, the crystals were grown repeatedly (three times) for purification. In this procedure the impurities tend to migrate to the extremities of the crystal during the growth, due to the segregation of impurities along the crystal. Thus, a better purity is expected to be found in the middle region. For each re-growth, the quartz tube was opened and two slice samples were taken from the crystals (Fig. 1). The "TOP" region refers to the upper ingot extremity (~5 mm), where most of the impurities migrate and it was taken for chemical analysis. The "MIDDLE" region was considered the prime region (~35 mm thick) of the crystal, assuming that a good uniformity in the impurity concentrations exists in the middle region of the ingot. Samplings (2 x 0.65 mm thick slices) were taken, adjacently, from the middle of the crystal, for chemical analysis and detector preparation. The "BOTTOM" corresponds to the lower ingot extremity, which has the cone shape (~ 20 mm thick).

A small amount of 50 mg were taken from the "TOP" region and the two 0.65 mm samplings of "MIDDLE" region to identify and determine the concentration of impurities present in each region.

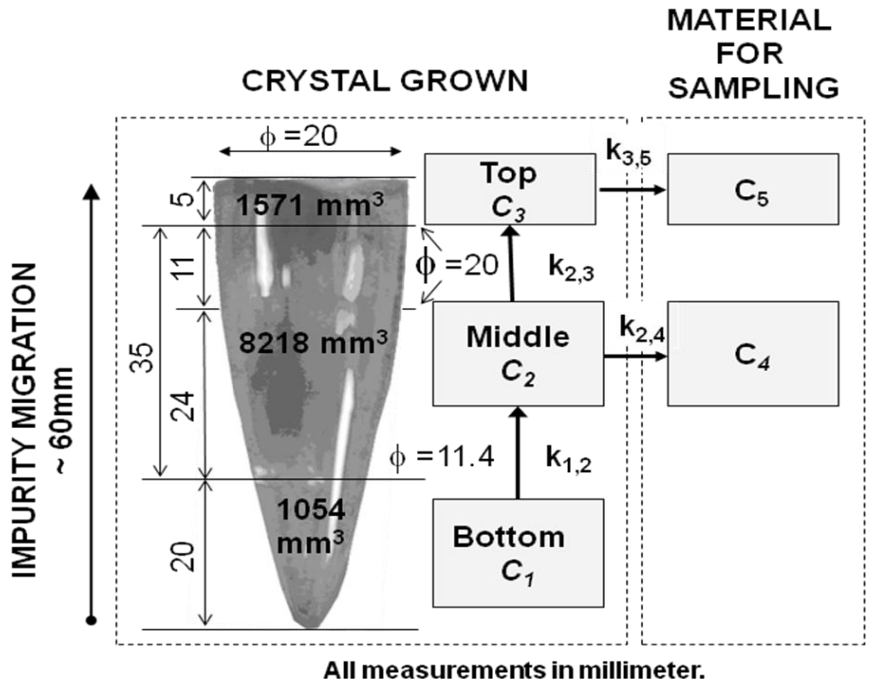

Figure1: compartmental model proposed to explain the migration of impurities in the TlBr crystal. The values of the constants $k_{i,j}$ are in Table 2.

The impurity concentrations of the samples, taken from slices after each growth, were measured in an ICP-MS (Inductively Coupled Plasma Mass Spectrometer, mod. Elan 6100 ICP-MS, Perkin Elmer, USA). Previously, samples had been digested in a mixture of nitric acid (65%, Merck) and hydrogen peroxide (30%, Merck) by closed-vessel microwave digestion. The ICP-MS instrumental operating conditions were optimized for the measurement of elements. Five impurity elements were found in the raw material: Barium (Ba), Calcium (Ca), Lithium (Li), Chromium (Cr) and Copper (Cu). The concentrations of Cu and Cr in the raw material were already in their limit of detection (0.02 ppm for Cu and 0.04 ppm for chromium).The sample concentrations were determined through calibration with certified single reference material. The samples were measured in 10 replicates and the results represented by the arithmetic mean and the standard deviation (mean ± sd). The *Kruskal-Wallis One Way Analysis of Variance on Ranks* was applied to identify significance differences among the crystal impurity concentrations, compared to those found in the raw salt. The statistical calculations were performed with the *Sigma Stat for Windows Version 1.0* (Jandel Co. USA). The impurity were expressed in parts per million (ppm).

The theory of compartments was used as a mathematical model to explain and to fit the data of the impurity concentration as a function of the crystal growth repetition number. In the theory of compartmental analysis, it is assumed that the variation in the contents of the ***i***th-compartment C_i (here C_i = impurity concentration), as a function of the variable ***x*** (here ***x*** = number of growth repetitions) may be equated as:

$$\frac{dC_i(x)}{dx} = -\sum_{i=1;i\neq j}^{N} k_{i,j} \cdot C_i(x) + \sum_{j=1;j\neq i}^{N} k_{j,i} \cdot C_j(x) \quad (1)$$

where $\boldsymbol{k_{i,j}}$ is the constant fraction of the impurity migration from the compartment (crystal region) $\boldsymbol{i}$ to compartment $\boldsymbol{j}$, $\boldsymbol{k_{j,i}}$ is the constant fraction of the impurity migration from the compartment $\boldsymbol{j}$ to compartment $\boldsymbol{i}$ and $\boldsymbol{N}$ is the total number of compartments. Especially, in this work N=5 and the constants $\boldsymbol{k}$ are expressed as $\boldsymbol{x^{-1}}$, i.e., the inverse of Bridgman growth repetition number.

The compartmental model proposed in this work, to explain the migration of impurities, is shown in Fig. 1. The $\boldsymbol{C_1}$ compartment ($\boldsymbol{V_{C1}}$ = 1054 mm^3) is assumed physically as being the bottom conical region which extends from zero to 20 millimeters in thickness (ϕ_{minor} = 2.2 mm, ϕ_{major} = 11.4 mm). The $\boldsymbol{C_2}$ compartment ($\boldsymbol{V_{C2}}$ = 8218 mm^3) is the middle region with 35 mm thick, being 24 mm in the conical region (ϕ_{minor} = 11.4 mm, ϕ_{major} = 20 mm) and 11 mm in the cylindrical region (ϕ = 20 mm). The $\boldsymbol{C_3}$ compartment ($\boldsymbol{V_{C3}}$ = 1571 mm^3) corresponds to the top cylindrical region with 5 mm thick (ϕ = 20 mm). The $\boldsymbol{C_4}$ and $\boldsymbol{C_5}$ compartments are located outside of the crystal region. They represent the material taken from the crystal for analysis. The accumulative $\boldsymbol{C_4}$ compartment corresponds to the 1.3 mm thick slice samples removed from $\boldsymbol{C_2}$, at 1st, 2nd and 3th growth used for chemical analysis and detector spectrometry characterization. The accumulative $\boldsymbol{C_5}$ compartment refers to the 5 mm thick slice samples removed from $\boldsymbol{C_3}$, at 1st, 2nd and 3th growth, to remove the top region where the impurities tend to migrate.

The core of this model, i.e., the $\boldsymbol{C_1}$, $\boldsymbol{C_2}$ and $\boldsymbol{C_3}$ compartments, can be defined, mathematically, as the first order differential equation system shown as follows.

$$\begin{aligned}
&\frac{dC_1}{dx} = -k_{1,2} \cdot C_1 \\
&\frac{dC_2}{dx} = +k_{1,2} \cdot C_1 - (k_{2,3} + k_{2,4}) \cdot C_2 \\
&\frac{dC_3}{dx} = +k_{3,5} \cdot C_3
\end{aligned} \qquad \begin{aligned}
&C_{1,0} = C_{2,0} = C_{3,0} = \text{The impurity concentration} \\
&\text{in raw material (Table 2) and } C_{4,0} = C_{5,0} = 0
\end{aligned} \quad (2)$$

Rewriting the equation system (2) in the matrix notation and assuming the algebraic feature $\sum_{i=1;i\neq j}^{N} k_{i,j} = k_{i,i}$, with the intent of achieving uniformity in the indexes of the array elements, we have:

$$\begin{bmatrix} -k_{1,1} & 0 & 0 \\ k_{1,2} & -k_{2,2} & 0 \\ 0 & k_{2,3} & -k_{3,3} \end{bmatrix} \cdot \begin{bmatrix} C_1 \\ C_2 \\ C_3 \end{bmatrix} = \begin{bmatrix} dC_1/dx \\ dC_2/dx \\ dC_3/dx \end{bmatrix} \quad (3)$$

By applying the Laplace transform [13] in (3) and inverting the [k] matrix:

$$\begin{bmatrix} \overline{\overline{C_1}}(s) \\ \overline{\overline{C_2}}(s) \\ \overline{\overline{C_3}}(s) \end{bmatrix} = \frac{1}{\Delta} \cdot \begin{bmatrix} (s+k_{2,2}) \cdot (s+k_{3,3}) & 0 & 0 \\ k_{1,2} \cdot (s+k_{3,3}) & (s+k_{1,1}) \cdot (s+k_{3,3}) & 0 \\ k_{1,2} \cdot k_{2,3} & k_{2,3} \cdot (s+k_{1,1}) & (s+k_{1,1}) \cdot (s+k_{2,2}) \end{bmatrix} \cdot \begin{bmatrix} C_{1,0} \\ C_{2,0} \\ C_{3,0} \end{bmatrix} \quad (4)$$

where, $\overline{\overline{C_i}}(s) = \mathcal{L}(C_i(x))$ the Laplace transformation of $\boldsymbol{C_i(x)}$ by changing the '$\boldsymbol{x}$ variable' to one in 's-space' and $\Delta = (s+k_{1,1}) \cdot (s+k_{2,2}) \cdot (s+k_{3,3})$.

$$\begin{bmatrix} \overline{\overline{C_1}}(s) \\ \overline{\overline{C_2}}(s) \\ \overline{\overline{C_3}}(s) \end{bmatrix} = \begin{bmatrix} \dfrac{(s+k_{2,2}) \cdot (s+k_{3,3})}{(s+k_{1,1}) \cdot (s+k_{2,2}) \cdot (s+k_{3,3})} \cdot C_{1,0} \\ \dfrac{k_{1,2} \cdot (s+k_{3,3}) \cdot C_{1,0} + (s+k_{1,1}) \cdot (s+k_{3,3}) \cdot C_{2,0}}{(s+k_{11}) \cdot (s+k_{2,2}) \cdot (s+k_{3,3})} \\ \dfrac{k_{1,2} \cdot k_{2,3} \cdot C_{1,0} + k_{2,3} \cdot (s+k_{1,1}) \cdot C_{2.0} + (s+k_{1,1}) \cdot (s+k_{2,2}) \cdot C_{3,0}}{(s+k_{11}) \cdot (s+k_{2,2}) \cdot (s+k_{3,3})} \end{bmatrix} \quad (5)$$

Finally, applying the inverse of Laplace transformation: $C_i(x) = \mathcal{L}^{-1}(C_i(s) = \frac{P_i(s)}{Q(s)})$, using the Heaviside algorithm where $\boldsymbol{Q(s)=\Delta}$ and $\boldsymbol{P_i(s)}$, the numerator elements of the matrix product (6), then we have:

$$C_1(x) = C_{1,0} \cdot e^{-k_{1,1} \cdot x} \quad (6)$$

$$C_2(x) = \frac{k_{1,2} \cdot C_{1,0}}{k_{2,2} - k_{1,1}} \cdot e^{-k_{1,1} \cdot x} + (\frac{k_{1,2} \cdot C_{1,0}}{k_{1,1} - k_{2,2}} + C_{2,0}) \cdot e^{-k_{2,2} \cdot x} \quad (7)$$

$$\begin{aligned} C_3(x) = {} & \frac{k_{1,2} \cdot k_{2,3} \cdot C_{1,0}}{(k_{2,2} - k_{1,1}) \cdot (k_{3,3} - k_{1,1})} \cdot e^{-k_{1,1} \cdot x} \\ & + (\frac{k_{1,2} \cdot k_{2,3} \cdot C_{2,0}}{(k_{1,1} - k_{2,2}) \cdot (k_{3.3} - k_{2,2})} + \frac{k_{2,3} \cdot C_{2,0}}{k_{3,3} - k_{2,2}}) \cdot e^{-k_{2,2} \cdot x} \\ & + (\frac{k_{1,2} \cdot k_{2,3} \cdot C_{3,0}}{(k_{1,1} - k_{3,3}) \cdot (k_{2.2} - k_{3,3})} + \frac{k_{2,3} \cdot C_{2,0}}{k_{2,2} - k_{3,3}} + C_{3,0}) \cdot e^{-k_{3,3} \cdot x} \end{aligned} \quad (8)$$

The two end line compartments $\boldsymbol{C_4}$ and $\boldsymbol{C_5}$ have their cumulative impurities determined as:

$$C_4(x) = k_{2,4} \cdot \int_{x=0}^{x} C_2(x) dx \quad (9)$$

$$C_5(x) = k_{3,5} \cdot \int_{x=0}^{x} C_3(x) dx \quad (10)$$

Summarizing, $C_i(x)$ is the experimental concentration of impurities in the crystal region i after the x^{th} repetition of crystal growth, $C_{i,0}$ is the initial condition measured, experimentally, in raw material and $k_{i,j}$ is the constant migration of impurity, which is determined by the nonlinear least squares method. In this study, the compartmental calculations were made with Anacomp software [14,15,16].

The crystalline quality of the TlBr crystal was analyzed by X-ray diffraction (XRD). X-ray diffraction patterns were obtained in a Siemens (D5005) Diffractometer CuKα radiation (2θ ranging from 20° to 60º). The two sample slices from the middle crystal were prepared as a detector according to procedures described previously [7, 17]. The crystal was sliced in wafers, cut transversally to direction (110), using a diamond saw and lubricated with glycerine during the process. Crystals were cut slowly to have less damage and smaller depths in the resulting layers. The polishing, cleaning and electrode paintings were made, subsequently, without pause to avoid humidity deposition. The electrodes were made with colloidal carbon painting, Viatronix[TM]. The final dimensions of the crystal wafers were, approximately, 20 mm diameter and 0.65 mm thickness. The detectors were made with a central electrode (anode), plus a ring electrode surrounding the anode electrode. The anode electrode diameter is about 3 mm and the ring electrode is around 4 mm internal diameter plus approximately 10 mm external diameter. The area for each electrode was defined from the painting mask electrode area and the thickness with a micrometer. Fig. 2 shows a schematic diagram of the detector and its connection to the preamplifier. The output from A250F charge sensitive preamplifier was connected to a 450 EG&G Ortec Research Amplifier at 10 μs shaping time and to EG&G 918A Multichannel Analyzer, to obtain the pulse height spectra. TlBr crystal detectors were excited under a 59 keV ^{241}Am gamma source, biased with 400 V. For resistivity measurements, the ring electrodes were disconnected and the bias current measured with a 619 Keithley Multimeter. All measurements were carried out at room temperature, 24 ± 2 °C.

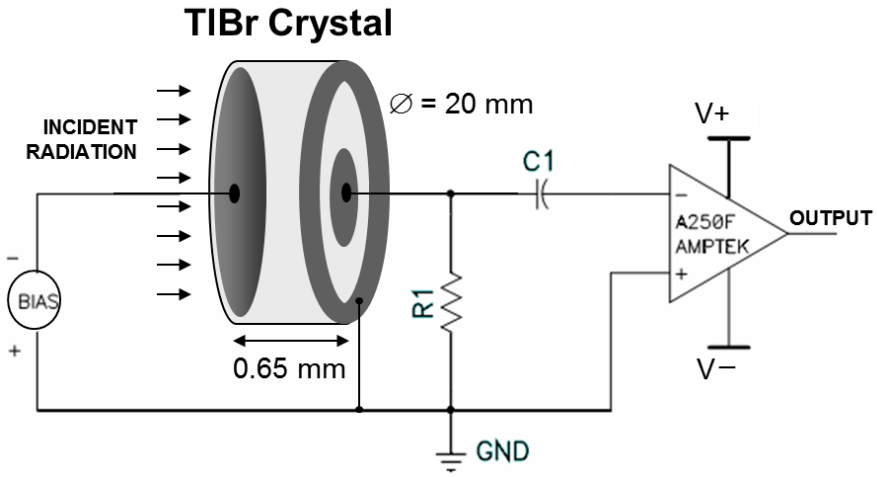

Figure 2: TlBr detector and preamplifier connections.

3. RESULTS AND DISCUSSION

The X-ray diffraction pattern of TlBr salt exhibited a complete set of reflections (Fig. 3 (a)), while the typical X-ray diffraction pattern of TlBr crystals grown in this work presented only a reflection line (Fig. 3(b)). The diffractogram indicates that the crystal is preferentially oriented in the (110) direction (Fig.3 (b)). It is worthwhile to observe that there was no other crystalline phase in the grown crystal since all detected peaks corresponded to the TlBr peaks oriented in the (110) direction. These results are in agreement with the literature [4,10].

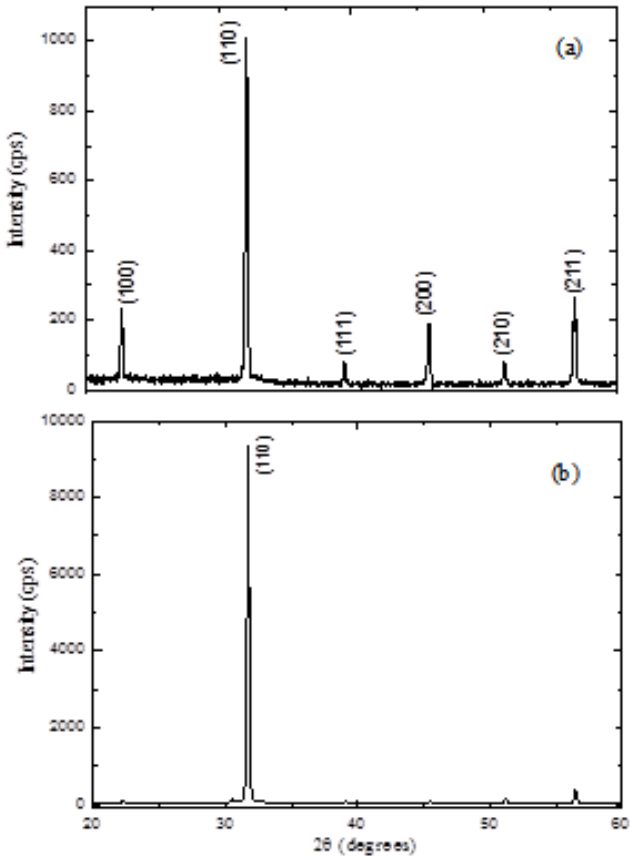

Figure 3: X-ray diffraction of TlBr powder (a) and TlBr crystal (b).

In the classical approach, to determine the calculation of the segregation coefficient *k*, some idealized hypothesis are assumed [18]: (i) the concentration of the impurity in the raw material is constant in all the extension of its distribution in the crucible; (ii) the ingot cross section is a constant; (iii) the segregation coefficient is constant along the ingot length; (iv) the initial concentration in each *i* region of the ingot corresponds to the sum of the entire ingot, divided by the number of region sections; (v) the ingot length should be greater than the melting zone length, in order to drag impurities based on solubility differences of the solid-liquid phase. If all these conditions are met, then the predictable mathematical model described in equation (11) may be used to calculate the concentration C_i after zone refining.

$$C_i = C_0 \times [1 - (1-k) \times e^{-k \cdot \frac{i}{l}}] \quad (11)$$

where: C_i is the concentration of the impurity in the *i*-th position along the ingot; C_0 is its initial concentration; *k* is the segregation coefficient and *l* is the melting zone length.

Due to the experimental particularities of the Bridgman purification used in this work, the following requirements mentioned previously are not established: 1st) in the crystal growth by the Bridgman technique, the raw material needs to be fully melted previously, what is in divergence with the hypothesis number (v); 2nd) in order to promote the nucleation, the growth crucible should be, preferably, cone-shaped, disregarding the hypothesis number (ii); 3th) due to the methodology applied, at each full melting, a fraction of the impurities, located in the top region, can recirculate by the Brownian movement, thereby reducing the efficiency of purification. To avoid this effect and to improve the quality of the purification process, the crucible of growth is opened and the upper portion of the crystal is cut and removed. Besides, to evaluate the effect of the impurities on the crystal performance as a radiation detector, samples were taken from the middle of the crystal, considered the prime region. Thus, due to these restrictions the mathematical model based on zone refining, described by the equation (11), is not suitable.

The theory of compartments is a powerful tool for analysis of kinetic phenomena, migration and transport of molecules and their chemical transformations. This form of deterministic analysis involves dividing the used system into a number of interconnected compartments, where a compartment is defined as any structural, functional, chemical or physical subdivision of a system. A basic assumption is that the analyte is uniformly distributed throughout the compartment. Therefore, this modeling theory is less restrictive than the model of equation (11), being more suitable for analyzing the data of this work. The compartmental model, proposed to explain the migration of impurities as a function of the x^{th} repetition of Bridgman growth, is shown in Fig. 1. The *k* parameters are the migration constants of the impurities from the region *i* to the region *j*. Compartment C_5 represents the accumulative quantities of impurities taken from the top crystal region (5mm). Compartment C_4 represents the accumulative impurity amount in slice samples (1.3 mm) removed from the middle crystal region, to be used as a radiation detector and for chemical analysis. The basic assumptions applied to the formulation of model described in Fig. 1 and equations (6-10) were: (i) the segregation coefficient $k > 1$, i.e., the measured impurities are more soluble in the molten fraction of the crystal; (ii) initially, the impurity concentrations in the three regions (compartments), 1 to 3, are equal to the salt used as raw material and the initial concentration in compartments 4 and 5 are both equal to zero; (iii) the migration coefficients $k_{i,j}$ is a constant, independently of the crystal growth repetition number *x*, i.e., the quantity of impurities that migrate from region *i* to region *j* is proportional to their concentration in region *i* and, finally, (iv) $k_{1,2} = k_{2,3}$. This algebraic feature allows a reduction in the number of variables to be determined by the nonlinear least-square method [19], moreover, this hypothesis is in agreement with the same rule (hypothesis number (iii)), used in the formulation of the zone refine model (the *k* without index in the equation (11)). The constants $k_{2,4}$ and $k_{3,5}$ depend on the size of the sliced material removed from the crystal and were numerically estimated by the fitting regression process.

The concentration of three ions (Ca, Ba and Li) found in the crystal grown three times sequentially for the two salts are presented in Table 1 and Fig. 4. Comparisons among initial impurities from two salts (raw materials) suggest that salt 1 has less Ba (5.46±0.10 ppm) than salt 2 (9.64±0.11 ppm), while both salts have similar concentration of Ca (8.99±0.12 ppm for salt 1 versus 7.69±0.09 ppm for salt 2) and Li (2.39±0.10 ppm for salt 1 versus 1.92±0.10 ppm for salt 2).

Table 1: three impurity concentrations (ppm) in the TlBr salt and in the top and middle regions of the TlBr crystal, by ICP-MS. The values represents the mean one standard deviation (N=10 samples).

TlBr ORIGIN			CRYSTAL REGION	IMPURITIES ELEMENTS (ppm) Ba	Ca	Li
SALT 1	**Bridgman Growth Step**		**RAW MATERIAL**	**5.46 ± 0.10**	**8.99 ± 0.12**	**2.39 ± 0.10**
		First	**TOP**	5.36 ± 0.12	8.58 ± 0.13	2.34 ± 0.14
			MIDDLE	4.93* ± 0.12	8.28* ± 0.07	2.05 ± 0.12
		Second	**TOP**	6.38* ± 0.13	8.49 ± 0.10	3.00* ± 0.12
			MIDDLE	6.09* ± 0.11	8.16* ± 0.13	3.04* ± 0.11
		Third	**TOP**	5.49 ± 0.11	8.13* ± 0.09	2.76 ± 0.11
			MIDDLE	3.05* ± 0.15	6.88* ± 0.12	1.88* ± 0.12
SALT 2	**Bridgman Growth Step**		**RAW MATERIAL**	**9.64 ± 0.11**	**7.69 ±0.09**	**1.92 ± 0.10**
		First	**TOP**	9.25* ± 0.09	8.03* ± 0.09	1.61* ± 0.12
			MIDDLE	9.10* ± 0.11	7.63* ± 0.10	1.60* ± 0.07
		Second	**TOP**	9.11* ± 0.12	7.62 ± 0.12	1.54* ± 0.11
			MIDDLE	8.96* ± 0.10	7.49 ± 0.012	1.40* ± 0.06
		Third	**TOP**	9.02* ± 0.09	7.45* ± 0.11	1.57* ± 0.09
			MIDDLE	8.68* ± 0.08	6.96* ± 0.12	1.33* ± 0.12

* There is a statistical difference between sample value and the initial concentration of raw salt ($p < 0.05$).

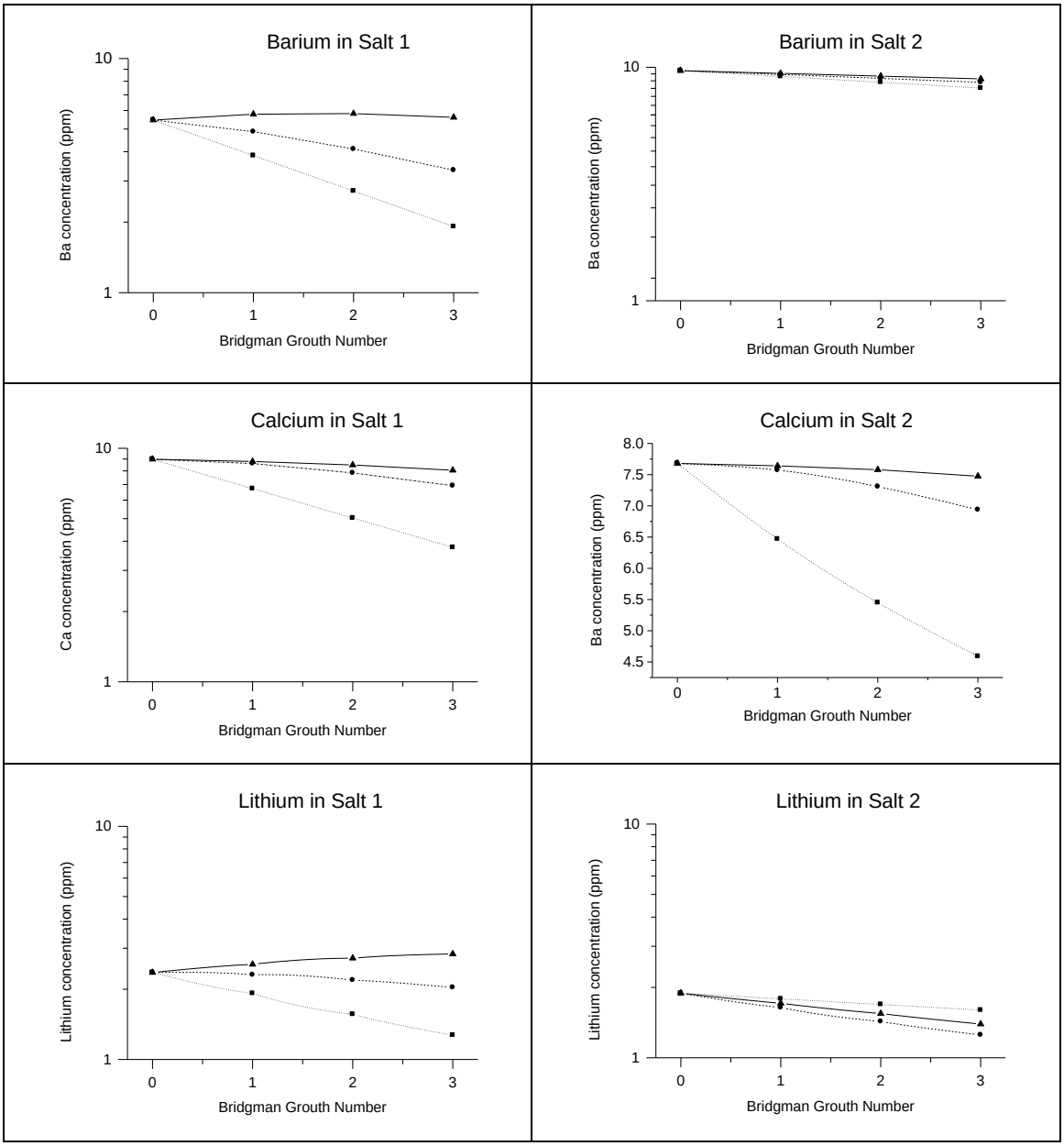

Figure 4: Concentration of impurity ions in different regions of crystals. ■ bottom region = compartment C_1, ● middle region = compartment C_2 and ▲ top region = compartment C_3. Values were calculated theoretically from model described in Fig. 1 and equations (7), (8) and (9).

For salt 1, after the first purification, the amount of impurities in the top region was not, significantly, different from the raw salt. However, for salt 2, significant differences were found for all three impurity elements in the crystal top region. In the case of the crystal middle region, a significant difference in the crystal impurity concentrations was observed for almost all impurities, compared to those found in the raw material (salts 1 and 2).

According to Table 1, for salt 1, the reduction level of the impurities in the crystal middle region, after the third growth, was of 44% (1-(3.05/5.46)) for Ba, 23% (1-(6.88/8.99)) for Ca and 21% (1-(1.88/2.39)) for Li. On the other hand, for the second salt, the results were worse, with 10% (1-(8.68/9.64)) for Ba, 9% (1-(6.96/7.69)) for Ca and 31% (1-(1.33/1.92)) for Li. Comparing the averages of $k_{1,2}=k_{2,3}$ (Table 2) for the two salts, similar results can be reached. It should be emphasized that, in the compartmental theory, there is not a rigorous commitment that k parameter be equal among the regions. However, for the same raw salt, the $k_{1,2}=k_{2,3}$ values found were close to each other, thus this assumption may be assumed. The difference in the mean values of these two groups (0.28 ± 0.07 vs 0.094 ± 0.07) is greater than what could be expected by chance, hence, there is a statistically significant difference between salts 1 and 2 ($P = 0.0271$). These results suggest that some unknown factors, present in salt 2, slow down the separation of impurities along the crystal and, consequently, the choice of the commercial raw salt should be made experimentally, independently of their nominal declaration of purity.

Table 2: Impurity migration coefficients.

Impurities	Transfer Coefficient	TlBr Powder 1 (x^{-1})[a]	TlBr Powder 2 (x^{-1})[a]
	k1,2 = k2,3	0.35 ± 0.01[b]	0.057 ± 0.003[b]
Barium	**k2,4**	0.074 ± 0.013[b]	0.037 ± 0.003[b]
	k3,5	0.26 ± 0.01[b]	0.083 ± 0.003[b]
	k1,2 = k2,3	0.29 ± 0.09[b]	0.17 ± 0.02[b]
Calcium	**k2,4**	0.0076 ± 0.0463[b]	0.00070 ± 0.00887[b]
	k3,5	0.311 ± 0.086[b]	0.18 ± 0.02[b]
	k1,2 = k2,3	0.21 ± 0.51[b]	0.056 ± 0.356[b]
Lithium	**k2,4**	0.004 ± 0.200[b]	0.14 ± 0.02[b]
	k3,5	0.12 ± 0.45[b]	0.15 ± 0.34[b]
Mean ± SD	**k1,2 = k2,3**	**0.283 ± 0.029**	**0.094 ± 0.066**

[a] x = Number of repeated Bridgman growth.
[b] Regression asymptotic error (the calculated error in the last iteration).

The model shown in Fig. 1 is valuable for quality control purpose. In such case, the $k_{i,j}$ parameters, which are associated to the impurity migration efficiency, can be an important auxiliary tool to design, optimize and explain the results and processes involved in the purification of raw salt used to grow crystals. For example, to understand the rise in the concentration of impurities in the crystal middle region increased in the second Bridgman growth (Figs. 4 and 5), although seeming a contradiction, this occurrence can be predicted and quantified by the compartmental analysis. As shown in Figure 4, the impurities concentration $C_2(x = 2) \sim 110\%$, in the middle of the crystal, is greater than that found in the raw material ($C_{2,0} = 100\%$). The proposed model, (Fig. 1), provides the comprehension of this effect, since it is capable to forecast that the impurities located in the prior region migrate to the subsequent region, contributing to the increase of their concentration. Thus, the parameter $k_{i,j}$ is valuable to represent the effectiveness of the purification technique. Moreover, the

model may be useful to predict the repetition number of Bridgman growths required to reduce the impurities to a level, for example, of 10% the raw salt (C_0=100%). In the present work, approximately, 10 repetitions of the Bridgman growth would be necessary (Fig. 5) to achieve this requirement.

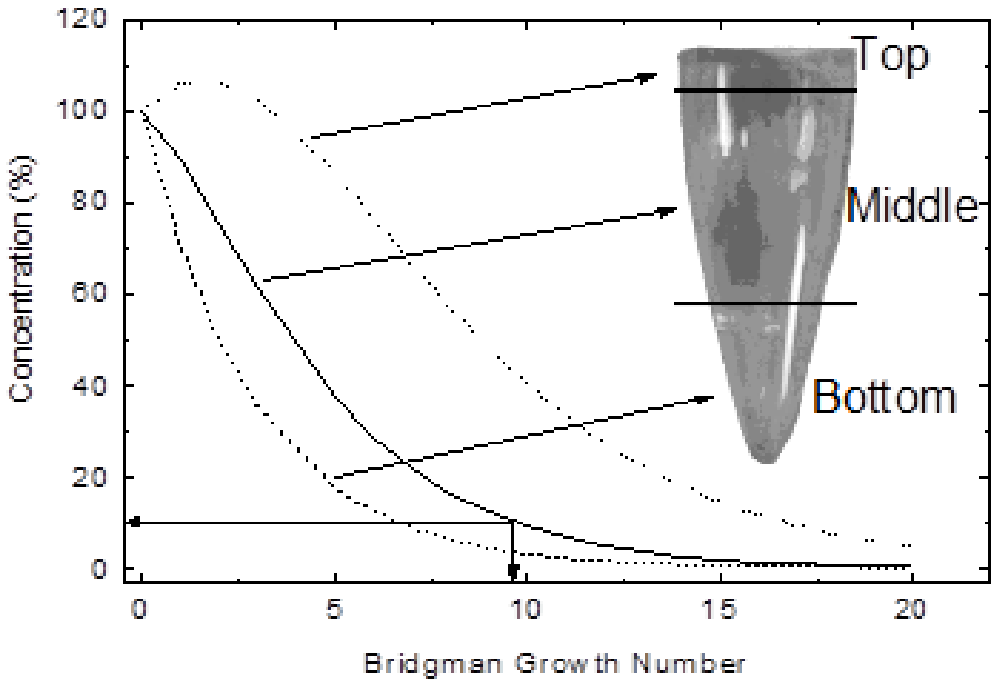

Figure 5: Predictive concentration (%) for the salt 1 as a function of repetition number of Bridgman growth, curves calculated from the model of Fig. 1 and equations (7), (8) and (9). To achieve 10% of initial concentration in the crystal middle region, approximately, 10 steps are required.

For the purpose of analyzing the effectiveness of the purification process, a spectrometric analysis was performed and the results were compared with the efficiency of the purification (Fig. 6). The pulse height spectra obtained suggest a significant improvement in their profiles when the purification number is increased. For the TlBr crystal grown once, it was not possible to observe the photopeak profile because the pulses generated fall in the electrical noise region. For the TlBr grown twice, it can be observed only the photopeak of 59 keV of ^{241}Am gamma source. For the third grown crystal, some ranges of energy below 59 keV can be observed. Both starting materials (salt 1 and 2) show similar spectrum details, although the raw material of salt 1 shows, systematically, better results, mainly in terms of resistivity values (Table 3 and Fig. 7). The resistivity found in this work is similar to that described by Hitomi et al. [6].

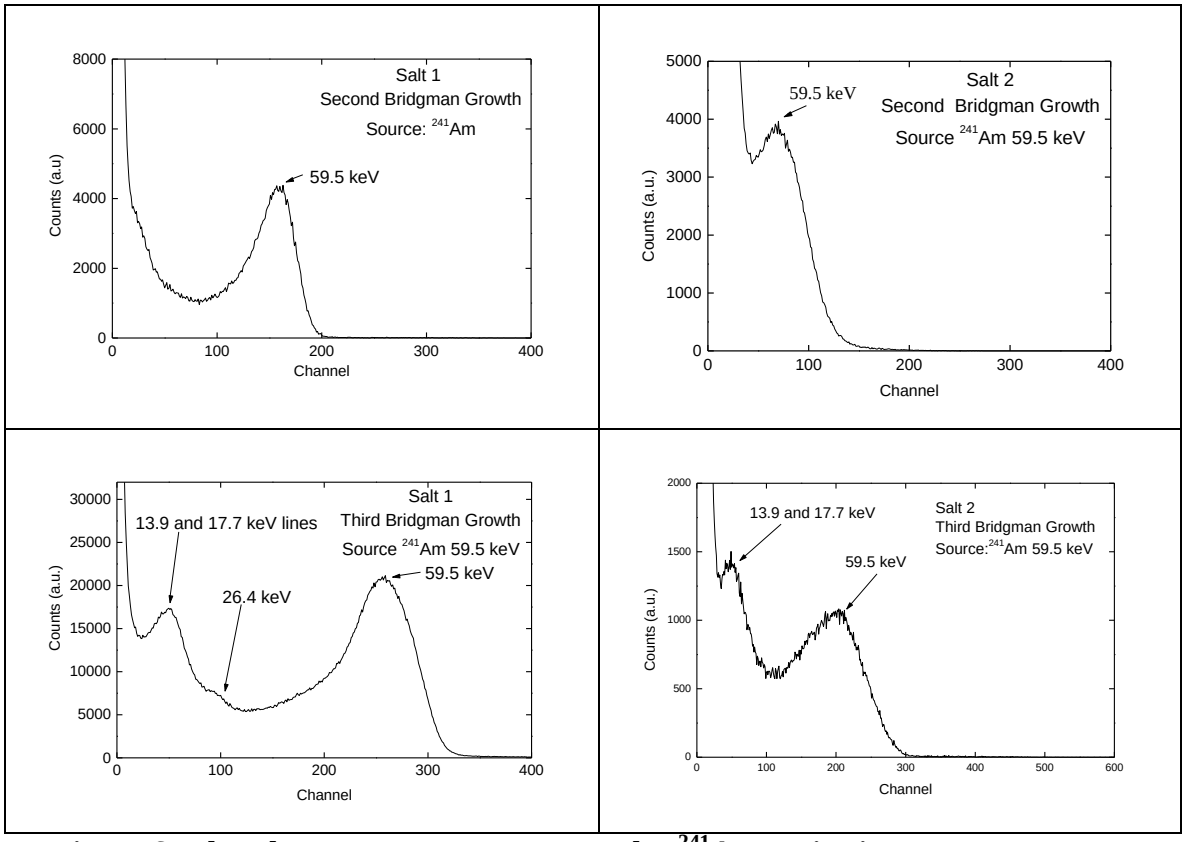

Figure 6: TlBr detector energy spectra under ^{241}Am excitations. Detectors were prepared using TlBr samples from the middle region of the crystals grown twice and three times.

Table 3: Resistivity values for TlBr detectors prepared from the crystal grown once, twice and three times, by the repeated Bridgman method. The samples used are from crystal middle region.

Bridgman Growth	Resistivity (10^9 Ωcm)	
	Salt 1	Salt 2
First	11.3 ± 9.5	2.17 ± 0.30
Second	47.5 ± 13.4	3.45 ± 0.45
Third	67.5 ± 21.9	6.72 ± 0.43

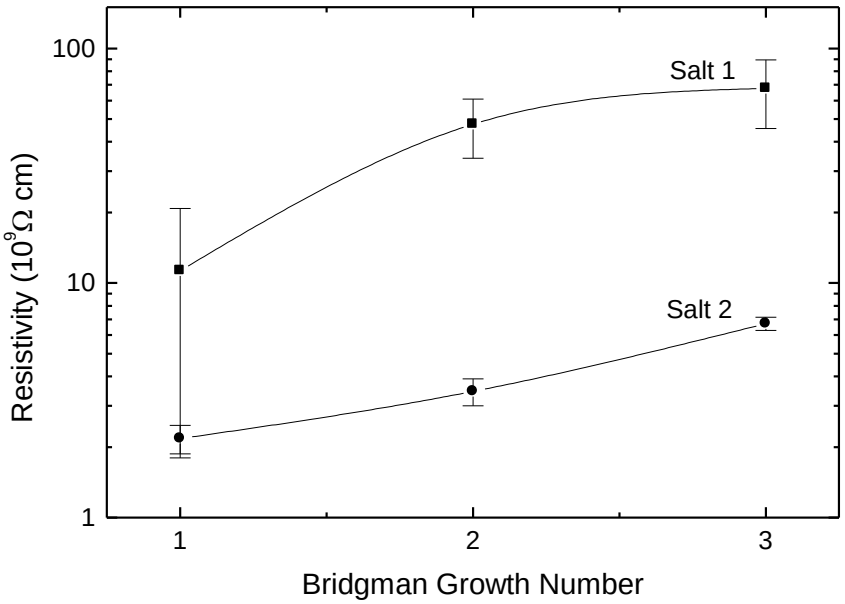

Figure 7: Resistivity of the TlBr detector from crystal middle region (slice ~ 0.65 mm thick) as a function of the repetition number of Bridgman growth. The bar error represents one standard deviation (N=3 samples).

The resistivity curve showed a positive slope (Fig. 7), tending to achieve a plateau. Although both salts had, nominally, the same initial purity (99.99%), the crystals grown showed resistivity differences of, approximately, 10 times. The resistivity of the crystals from salt 1 presented values 10 times higher than crystals from salt 2 (Fig. 7 and Table 3). There is evidence that salt 1 has better performance in all parameters studied: this fact could be associated with the resistivity of crystals. In fact, the lowest resistivity of the crystals produced with salt 2 could be correlated with its lower performance. However, comparing the spectrometric performance, while the crystal from salt 1-first growth (high resistivity) did not show any detail spectrum, in contrast, salt 2-second and third growths (low resistivities) presented good detail spectra (Fig.6). This fact suggests that the resistivity did not seem to have a fundamental role to characterize the spectrum quality of the crystal. Hitomi et al.[6] described similar observation on their result of resistivity measurements correlated to the number of zone-refining passes carried out in the TlBr purification. Further studies should be carried out to elucidate these results.

4. CONCLUSIONS

The repeated Bridgman method was efficient to purify the TlBr crystals and to improve their performance as radiation detectors. A compartmental model defined by linear differential equations may be used to calculate the coefficients for the migration of impurities. This is useful for predicting the number of repetitions in Bridgman growth needed to achieve a desirable concentration value. The resistivity showed a positive slope, tending to reach a plateau after the third growth. Above 3 MΩ, the resistivity of the TlBr crystal seems to not affect the spectrometry quality of the detector.

ACKNOWLEDGMENTS

The authors are grateful to FAPESP, CNPq and CNEN for the financial support. R. A. Santos and J.F.T. Martins express their gratitude to CNEN for the fellowships.

REFERENCES

1. D.S Macgregor & H. Hermon, "Room-temperature compound semiconductor radiation detectors" *Nuclear Instruments and Methods in Physics Research* A, **Vol.395**, pp.101-124 (1997).
2. I.B. Oliveira, F.E. Costa, J.F.D. Chubaci, M.M Hamada, "Purification and preparation of TlBr crystals for room temperature radiation detector applications," *IEEE Transactions on Nuclear Science*, **Vol.51**, pp. 1224-1228 (2004).
3. K. Hitomi, M. Matsumoto, O. Muroi, T.Shoji, and Y. Hiratate, "Characterization of thallium bromide crystals for radiation detectors applications," *Journal of Crystal Growth*, V**ol. 225**, pp.129-133 (2001).
4. V. Kozlov, H. Andersson, V. Gostilo, M. Leskelã, A. Owens, M. Shorohov and H. Sipila, "Improved process for the TlBr single-crystal detector" *Nuclear Instruments and Methods in Physics Research* A **Vol.591**, pp.209-212 (2008).
5. M..S. Kouznetsov, I.S. Lisitsky, S.I. Zatoloka and V.V. Gostilo. "Development of the technology of growing TlBr detectors crystals" *Nuclear Instruments and Methods in Physics Research* A, **Vol.531**, pp.174-180 (2004).
6. K. Hitomi, T. Onodera, T. Soji. "Influence of zone purification process on TlBr crystals for radiation detector fabrication" *Nuclear Instruments and Methods in Physics Research* A **Vol.579**, pp.153-156 (2007).
7. C. L. Vieira, F. E. Costa, M.M. Hamada, "Effect of etching on the TlBr crystal surface and its radiation response", *In: International Nuclear Atlantic Conference, VIII ENAN Proceedings*, Santos, Brazil, September 30 – October 05, 2007.
8. J. Vaitkus, V. Gostilo, R. Jasinskaite, A. Mekys, A. Owens, S. Zatoloka and A. Zindulis, "Investigation of degradation of electrical and photoelectrical properties in TlBr crystals." *Nuclear Instruments and Methods in Physics Research* A **Vol.531**, no.1-2, pp.192-196 (2004).
9. I.B. Oliveira, F.E. Costa, P.K. Kiyohara, M.M. Hamada, "Influence of crystalline surface quality on TlBr radiation detector performance." *IEEE Transactions on Nuclear Science*, **Vol.52**, pp.2058-2062 (2005).
10. V. Kozlov, M. Kemell, M. Vehkamâki, and M. Leskelã, "Degradation effects in TlBr single crystals under prolonged bias voltage" *Nuclear Instruments and Methods in Physics Research* A **Vol.576**, no.1, pp.10-14 (2007).
11. T. Onodera, K. Hitomi, T. Shoji, "Spectroscopic performance and long-term stability of thalium bromide radiation detectors" *Nuclear Instruments and Methods in Physics Research A* **Vol.568**, no.1, pp.433-436 (2006).
12. K. Hitomi., T. Onodera, T. Shoji, Z. He. "Pixellated TlBr detectors with the depth sensing technique" *Nuclear Instruments and Methods in Physics Research* A **Vol.578**, no.1, pp.235-238 (2007).
13. M. Abramowitz & I.A. Stegun, *Laplace Transforms, ch.29, Handbook of Mathematical Functions with Formulas, Graphs and Mathematical Tables*, 9th printing, New York, Dover, 1972, pp. 1019 – 1030.
14. M. Berman. *The formulation and testing of models*, Ann NY Acad Sci 1963;108:182-94

15. A. Rescigno, G. Segre, *Drug and tracer kinetics*, Waltham, Mass., Blaisdell Pub. 234 pg Co, 1966.
16. C. H. Mesquita, *AnaComp – Compartmental Analysis Aided by Computer - User Manual*. Instituto de Pesquisas Energéticas e Nucleares. São Paulo, 1994.
17. F. E. Costa, C. H. Mesquita, M. M. Hamada, "Temperature Dependence in the Long-Term Stability of the TlBr Detector" *IEEE Transactions on Nuclear Science*, **Vol.56**, pp.1-6 (2009).
18. W.G. Pfann, , *Zone Melting*. New York, N.Y.: John Wiley, 1958.
19. P.R. Bevington, *Data Reduction and Error Analisys for The Physical Sciences*, McGraw-Hill, New York, U.S.A, pp. 204 – 246, 1969.